Materials Today Bio 15 (2022) 100272

Contents lists available at ScienceDirect

Materials Today Bio

journal homepage: www.journals.elsevier.com/materials-today-bio

Drug-loaded oleic-acid grafted mesoporous silica nanoparticles conjugated with α-lactalbumin resembling BAMLET-like anticancer agent with improved biocompatibility and therapeutic efficacy

Wei Pei [a,1], Ling Cai [b,1], Xing Gong [a,1], Li Zhang [a,1], Jiarong Zhang [a], Ping Zhu [a], Huijun Jiang [c], Chao Wang [a], Shoulin Wang [a,d,**], Jin Chen [a,b,d,e,*]

[a] Center for Global Health, School of Public Health, Nanjing Medical University, 211166, Nanjing, China
[b] School of Chemistry and Chemical Engineering, Southeast University, Nanjing, 211189, China
[c] School of Pharmacy, Nanjing Medical University, 211166, Nanjing, China
[d] The Key Laboratory of Modern Toxicology, Ministry of Education, School of Public Health, Nanjing Medical University, 211166, Nanjing, China
[e] Jiangsu Province Engineering Research Center of Antibody Drug, Key Laboratory of Antibody Technique of National Health Commission, Nanjing Medical University, Nanjing, 211166, China

ARTICLE INFO

Keywords:
Drug delivery
Mesoporous silica nanoparticle
BAMLET
α-lactalbumin
Protein corona

ABSTRACT

Despite its prominent therapeutic efficacy, chemotherapy has raised serious concerns due to the severe adverse effects and multidrug resistance evoked, which propels the search for safe and green therapeutic agents. BAMLET (bovine α-lactalbumin made lethal against tumor cell) is a well-known protein-based anticancer agent of selective tumoricidal activity. Here, we prepared oleic acid-modified mesoporous silica nanoparticles (OA-MSNs) conjugated with bovine α-lactalbumin, a lipoprotein complex resembling BAMLET formed on the surface of MSNs (MSN-BAMLET) to load the anticancer drug of docetaxel (DTX). Compared to that of OA-MSNs/DTX, the obtained MSN-BAMLET/DTX with a sustained and pH-responsive drug release behaviors exhibited good biocompatibility and enhanced cytotoxic effect against cancer cells. Moreover, the presence of lipoprotein complex in MSN-BAMLET contributed to the improved dispersion of the composite in solution and the inhibitory effect on the migration of cancer cells. Furthermore, the adsorption profiles of protein corona on the obtained nanoparticles were analyzed. It was found that the marked low amount and abundance of plasma proteins were adsorbed on the α-lactalbumin coated siliceous composite demonstrated its long circulation property. Finally, *in vivo* study showed that MSN-BAMLET/DTX contributed to the effective cancer ablation and the prolonged survival. Therefore, the constructed MSN-BAMLET of the mesoregular structure and peculiar tumoricidal effect provides a manipulable nanoplatform as drug nanocarrier for therapeutic applications.

1. Introduction

Despite its prominent tumoricidal effects to prolong the survival of cancer patients, the chemotherapy has raised considerable concerns due to their adverse effects, rapid blood clearance and low bioavailability during the cancer treatment [1–3]. For example, docetaxel (DTX), a member of taxane (PTX) family isolated from the Pacific yew tree of Taxus brevifolia [4,5], is the first-line anticancer drug towards a broad spectrum of cancers such as breast, prostate, and lung cancer [6–9]. Though DTX shows improved therapeutic potency as compared with that of paclitaxel but its poor aqueous solubility (3 μg/ml) may hamper its clinical utilizations. Additionally, the use of detergent of high concentration such as Tween-80 in the formulated DTX may cause severe side effects [10]. It is urgent to search for a green and safe strategy to improve the therapeutic efficacy of chemotherapy.

Owing to the peculiar effect of nanomaterials at the nano-sized level, the various drug delivery systems using nanocarriers including liposome, carbon nanotubes, micelle, protein conjugate and polymeric nanoparticles have been developed [11–13,71,72]. Among them, mesoporous silica nanoparticles (MSNs) of tailored meso-structure, high surface area

* Corresponding author. Center for Global Health, School of Public Health, Nanjing Medical University, 211166, Nanjing, China.
** Corresponding author. Center for Global Health, School of Public Health, Nanjing Medical University, 211166, Nanjing, China.
E-mail addresses: wangshl@njmu.edu.cn (S. Wang), jchen@njmu.edu.cn, okachen30@gmail.com (J. Chen).
[1] equal contribution.

https://doi.org/10.1016/j.mtbio.2022.100272
Received 8 March 2022; Received in revised form 22 April 2022; Accepted 26 April 2022
Available online 4 May 2022

and large pore volume possess superior advantages as drug delivery matrix [16–19]. Upon surface modifications of exterior and internal mesopores, stimuli-response and targeted drug delivery based on the use of MSNs were achieved [20,21]. Furthermore, the nontoxic nature of MSNs is desirable for biomedical applications [22–24].

HAMLET or BAMLET (human/bovine α-lactalbumin made lethal against tumor cells), the widely known anticancer agent, are formed as the lipoprotein complex [25]. Since HAMLET was firstly identified from human milk in 1995, these anticancer agents have been extensively studied due to their noticeable ability to kill diverse cancers cells and negligible cytotoxicity to normal cells [26,27]. Notably, as α-lactalbumin is a major protein of natural dietary nutrient, HAMLET/BAMLET is regarded as extremely safe anticancer agent [28–31]. Nevertheless, the scale-up preparation of HAMLET/BAMLET may involve labor-intensive work which may be an obstacle for the practical applications. A vast amount of clinical trials were conducted to prove the potent tumoricidal activity of HAMLET such as bladder cancer [32], human glioblastoma [33] and skin papillomas [30]. However, none of trials have been applied for the administration of endovascular injection due to the poor biocompatibility and strong hemolytic activity of BAMLET [34]. Consequently, it remains prudent for the clinical practice of BAMLET especially in the case of endovascular treatment.

In this study, inspired by our earlier study of successful grating oleic acids (OA) on the surface of rod-like mesoporous silica nanomaterials [35], we prepared a new OA-modified MSNs (OA-MSNs) to form conjugates with bovine α-lactalbumin (BLA), named as MSN-BAMLET, and compared their anticancer effect and biocompatibility with BAMLET. As protein loaded MSNs endows the composite with extended blood circulation and low surface potential to avoid the adsorption of serum proteins [36,37], we found that the constructed DTX-loaded MSN-BAMLET (MSN-BAMLET/DTX) exhibits good biocompatibility and enhanced cytotoxic effect against cancer cells compared to that of OA-MSNs/DTX. In addition, the sustained and pH-responsive drug release behaviors of MSN-BAMLET/DTX was identified, which is sufficient to inhibit the migration ability of cancer cells and increase the bioavailability of drug formulations. We further demonstrated that the α-lactalbumin coated MSNs adsorbed lowest amount and abundance of protein which may reduce its interaction with plasma proteins and realize the long circulation. According to the *in vivo* study of these nanoparticles, MSN-BAMLET/DTX exhibited the improved anticancer therapeutic effect as compared to that of OA-MSNs/DTX or DTX alone.

2. Experimental section

2.1. Materials

To minimize the batch difference of produced composites, mesoporous silica nanoparticle (MSNs) and amino-functionalized MSNs (MSNs-NH_2) were obtained from XFNANO industry. Bovine α-lactalbumin (calcium depleted, ≥85% purity) was purchased from Sigma-Aldrich. 1-(3-Dimethylaminopropyl)-3-ethylcarbodiimide (EDC), oleic acid, docetaxel, N-Hydroxysuccinimide (NHS) and 8-anilinonaphthalene-1-sulfonic acid (ANS) were from Shanghai Aladdin biochemical technology. Acetonitrile of HPLC-grade, anhydrous ethanol and dichloromethane were from Sinopharm Chemical Reagent. Dialysis membrane (molecular mass cutoff of 8–14 kDa) was obtained from Henghuibio technology development co., LTD. Fetal bovine serum (FBS), Dulbecco's modified Eagle's medium (DMEM), penicillin-streptomycin (10000 U/ml) were purchased from Gibco (Thermo Fisher Scientific). Cell counting kit-8 (CCK-8), JC-1 (5,5′,6,6′-tetrachloro-1,1′,3,3′-tetraethylbenzimidazoly l-carbocyanineiodide) and Mitochondrial membrane potential assay kit were purchased from MedChemExpress. Dithiothreitol (DTT), 4′, 6-diamidino-2-phenylindole (DAPI) and 0.25% trypsin-ethylenediaminetetraacetic acid (EDTA) were purchased from Beyotime Institute of Biotechnology. The assay solutions were prepared using deionized water. All other chemicals and reagents were of analytical grade unless otherwise specified.

2.2. Characterizations of prepared nanomaterials

Morphological properties of the nanoparticles were observed by scanning electron microscopy (SEM, JEOL, JSM-7900F) with a Lower Electron Detector (LED) at an acceleration voltage of 3.0 kV. All samples were coated with gold film before observed. Transmission electron microscopy (TEM, JEOL JEM-1010) was operated at an accelerating voltage of 80 kV and the sample size distribution was evaluated by Image J. Hydrodynamic diameter and Zeta-potential of the sample was recorded by Zetasizer Nano ZSP (Malvern Panalytical). To examine the modified functional group onto the samples, Fourier transform infrared (FT-IR) spectroscopy was performed on a FT-IR spectrometer (Nicolet Is 50, Thermo Scientific) in the range of 4000-400 cm^{-1}. Thermogravimetric analysis (TGA) was performed under air flow from 30 °C to 800 °C at a heating rate of 20 °C min^{-1} on a Pyris 1 DSC thermal gravimetric analyzer (USA, PerkinElmer).

2.3. Synthesis of OA-MSNs and MSN-BAMLET

To prepare OA grafted MSNs, 125 μL oleic acid was firstly dissolved in 5 ml ethanol and mixed with 100 mg EDC, 110 mg NHS as the coupling reagents to activate the carboxyl groups of OA. After mixing the solution under the stirring for 30 min at room temperature, 50 mg MSNs-NH_2 was added to the solution and the reaction mixture was incubated under gentle stirring for 12 h. OA-MSNs was collected by the centrifugation and washed with deionized water and ethanol for three times to remove unreacted OA, EDC and NHS.

A hydrothermal approach was used to produce the conjugates of α-LA and grafted unsaturated C18:1 oleic acid through the hydrophobic interaction and electrostatic attraction according to the previous study with some modifications [38,39]. First, 30 mg BLA was dissolved at 1 mM in 10 mM phosphate buffer at pH 8.0. Then, 15 mg OA-MSNs was added to the solution and vortexed for 10 s. This mixture was incubated at 45 °C in water bath for 15 min and centrifuged at 4 °C, 10000 rpm for 10 min to remove the unbound BLA. The final product was obtained by vacuum freeze-drying. Relative surface hydrophobicity was measured by using ANS. A solution containing 100 μg/ml ANS and 100 μg/ml BLA in PBS was incubated for 1 h at room temperature with ANS fluorescence measured at 350 nm excitation.

2.4. Loading of docetaxel on MSN-BAMLET

For DTX loading, a solvent evaporation method was performed. To examine the drug loading efficiency of the nanocarriers, MSNs, MSNs-NH_2, OA-MSNs were used to load DTX separately. Briefly, excessive DTX (25 mg) was dissolved in a closed container with 10 ml of dichloromethane. Then, 25 mg of nanocarriers were added to the as-obtained stock solution and stirred gently at 37 °C for 24 h. The solvents were permitted to volatilize to around 1 ml to form a progressively increased concentration of DTX, which may promote the adsorption of drug into mesopores [40]. The free DTX were removed by the centrifugation and washed with deionized water three times.

To measure the drug loading capacity of nanocarriers, MSNs/DTX, MSNs-NH_2/DTX and OA-MSNs/DTX were suspended in dichloromethane and ultrasonicated to release the drug followed by the suspension collection by the centrifugation at 13000 rpm for 10 min. This process

was repeated three times. The supernatant was collected and dried to remove the residual solvent. HPLC system with C18 column (4.6 × 150 mm, 5 μm) was employed to determine the drug concentration in the nanocarrier. The mobile phase consisted of acetonitrile and water (65/35, v/v) at flow rate of 1.0 ml/min, and the detection wavelength was set at 230 nm. The injection volume for drug analysis was 20 μL. The drug loading efficiency (LE) was calculated according to the equation [40]: LE (%) = Weight of DTX in nanoparticles/Weight of DTX loaded nanoparticles × 100.

2.5. In vitro drug release study

To study the *in vitro* drug release of DTX at different pH values, 1.5 ml of deionized water with MSN-BAMLET/DTX (3 mg) was sealed in a dialysis bag. The dialysis bag (molecular mass cutoff of 8–14 kDa) containing the mixture (0.5 ml) was immersed in 250 ml, 10 mM PBS (pH = 7.4 or 5.5) containing 0.1% Tween 80 and placed on a shaker at 37 °C. At specific time points, 0.5 ml solution was taken out and equivalent volume of the fresh medium was added back to the dialysate. The amount of DTX was quantified by the HPLC analysis.

2.6. Cell culture

Human cervical tumor cells (HeLa), human breast cancer cells (MCF-7), the rat basophil leukemia cells (RBL-2H3), the murine embryonic fibroblasts (3T3) were cultured with DMEM medium supplemented with 10% FBS and 1% penicillin-streptomycin. All cells were incubated at 37 °C in a humidified atmosphere containing 5% CO_2.

2.7. Cell viability assays

Cells were seeded in 96 well plates at a density of 4000 cells/well and grown for 24 h. The medium was removed and replaced with fresh medium containing different concentrations of nanocomposites. After 72 h incubation, cell viability was detected by the CCK-8 kit. Absorbance was measured at 450 nm on a microplate reader. The cells without materials treatment were used as the control.

2.8. Hemolysis assay

First, fresh rat red blood cells (RBCs) were washed with PBS three times and made up to 4% (v/v) concentration. Subsequently, 0.5 ml of RBCs solution was mixed with equivalent volume of nanocomposites at different concentrations. After 24-h incubation, the suspension was centrifuging at 5000 rpm for 5 min and the supernatant was transferred to 96-well plate, of which the absorbance was measured at 570 nm using a microplate reader. Triton X (0.2%) was prepared as a positive control (PC), and the erythrocyte suspension treated with PBS was used as a negative control (NC). The percentage of hemolysis was derived from the equation: hemolysis (%) = (sample absorbance – absorbance of NC)/(absorbance of PC – absorbance of NC) × 100. The measurement was conducted in triplicate.

2.9. Cell membrane integrity assay

The cellular membrane integrity assessment was performed according to the previous study with some modifications [41]. After 72 h incubation of cells in 96-well plates with the different concentrations of nanocomposites, the quantity of nucleic acid released from the damaged HeLa cells was determined by measuring the absorbance of the supernatant at 260 nm. The cells without materials treatment were used as the control.

2.10. Cellular uptake of nanomaterials

We performed the fluorescence imaging of HeLa cancer cells using a confocal laser scanning microscope (CLSM). Fluorescent dyes of DAPI were used to stain the nucleus and fluorescein isothiocyanate (FITC) were used to label MSN-BAMLET/DTX (ChinaPeptides, Shanghai). Briefly, MSN-BAMLET/DTX was dispersed in the distilled water and mixed with FITC solution for 12 h at 4 °C. Then, the mixture was sealed in a dialysis bag under stirring for 72 h to remove free fluorescent dyes to collect the yellow labeled product. The cells were co-cultured with MSN-BAMLET/DTX-FITC conjugate for 2, 4, 24 h, respectively.

2.11. Evaluation of mitochondrial function

HeLa cells were cultured at a density of 1×10^6 per well in 6-well plates for 24 h and treated with OA-MSNs/DTX, MSN-BAMLET/DTX, DTX (at the same drug concentration 25 ng/ml), BAMLET and MSN-BAMLET (at the same protein concentration 12.5 μM). After the treatment, cells were washed with PBS and stained with JC-1 before incubating at 37 °C for 30 min. Then cells were collected, washed twice with PBS and resuspended for flow cytometry analysis.

2.12. Apoptotic activity

HeLa cells were seeded in 6-well plates at a density of 1×10^5 cells per well. After 24 h culturing, cells were incubated with OA-MSNs/DTX, MSN-BAMLET/DTX and free DTX for 72 h. The cells without any treatment were used as the control. All of the cells were digested by trypsin (without EDTA) and washed three times. Then HeLa cells were stained with Propidium Iodide (PI) and Annexin-V-Fluorescein Isothiocyanate in the dark for 15 min at room temperature and analyzed via flow cytometry.

2.13. Wound-healing assay

HeLa cell lines were seeded in 6-well plates at a density of 5×10^5 cells per well and incubated until the bottom of plates was covered with cells. After drawing five parallel vertical lines using the pipette tip, the detached cells were washed with PBS for three times. The HeLa cells were treated with OA-MSNs/DTX, MSN-BAMLET/DTX and DTX, respectively. And then the migrations of different groups of cells were observed under the inverted fluorescence microscope. The images at different time points were taken and the scratched area of 0 h (S_0), 24 h (S_{24}), 48 h (S_{48}), 72 h (S_{72}) was measured by Image J. The groups without materials treatment were used as the control.

Migration rate (%) = $(S_0 - S_t)/S_0 \times 100$.

2.14. Zebrafish experiments

Zebrafish were used to evaluate the effects of chemotherapy *in vivo*. Fertilized zebrafish eggs were reared in a recirculating system at 28 °C with a 14-h light, 10-h dark photoperiod. The DiI (1,1′-Dioctadecyl-3,3,3′,3′-tetramethylindocarbocyanine perchlorate) labeled HeLa cell line was injected into the yolk space of zebrafish embryos [42]. The eggs were immersed in DTX, OA-MSNs/DTX, and MSN-BAMLET/DTX solutions containing 12.5 ng/ml DTX, respectively. Under a fluorescent microscope, tumor development and invasion were observed on a daily basis. The experiments were approved by the Animal Ethics Committee of Nanjing Medical University.

2.15. Protein corona analysis

1 mg of each sample was suspended in 1 ml of PBS containing 10% FBS, similar to the amount of FBS usually used for cell culture. The dispersants were left in microtubes for 2 h at 37 °C to allow for protein adsorption and then protein-covered nanoparticles (NPs) were pelleted by centrifugation (13000 rpm 10 min) followed by washing in PBS buffer three times. The supernatant was discarded and the NP pellet was resuspended in 25 μL PBS. 10 μl of 4 × sample buffer and 5 μL of 4.8 M dithiothreitol were added to the NP pellet, followed by incubation at 70 °C for 1 h with shaking to release the adsorbed proteins. Desorbed proteins were characterized by sodium dodecyl sulfate polyacrylamide gel electrophoresis (SDS-PAGE) [43].

2.16. Tumor model establishment

Female BALB/c nude mice (6 weeks, ~17 g SPF mice) were used for the study. All mice were housed in a sterile animal room with a 12-h light–dark cycle, a constant ambient temperature of 21 °C, and a relative humidity of 40–70%. Food and water are freely available to all mice. All of our experiments have been authorized by Nanjing Medical University's Animal Ethics Committee and are carried out in accordance with ethical guidelines. HeLa cells (1×10^6 in 50 μl PBS and 50 μl Matrigel) were subcutaneously transplanted into the back of mice, which was continuously bred till tumor volume reached ~100 mm^3. The tumor volume was dynamically monitored and calculated as (long diameter × short $diameter^2$)/2.

2.17. Anticancer activity in subcutaneous HeLa tumor-bearing mice

When the tumor volume reached 100 mm^3, all of the mice were randomly assigned to one of five groups (n = 6 per group) and intravenously injected with PBS, OA-MSNs/DTX, MSN-BAMLET/DTX, free DTX (at a DTX dosage of 2.5 mg/kg), or BAMLET (at the same protein concentration as MSN-BAMLET/DTX) once every three days. At the same time, tumor sizes were measured via vernier caliper and the mice's body weights were also recorded. At day 47, the experiment was ended and all of the mice were euthanized to harvest solid tumors and main organs, which were then accessed for histopathological analysis using hematoxylin-eosin (H&E), terminal deoxynucleotidyl transferase-mediated dUTP-biotin nick end labeling (TUNEL), and Ki67 staining. In addition, whole blood was collected from the orbital venous plexus for clinical chemistry analysis.

3. RESULTS and DISCUSSION

As shown in Fig. 1, to obtain MSN-BAMLET/DTX, we firstly grafted oleic acids onto the surface of amidated MSNs [35] followed by the conjugation of BLA to form the BAMLET-like complex with the core-shell structure and the encapsulation of DTX. The morphology of the prepared nanoparticles was observed by scanning electron microscopy (SEM) and transmission electron microscopy (TEM) (Fig. 2). Image J was used to analyze the size distribution by counting the diameter of 100 nanoparticles. The spherical silica composite of meso-regularity was apparently visualized in TEM and SEM observations (Fig. 2A, B, C) with

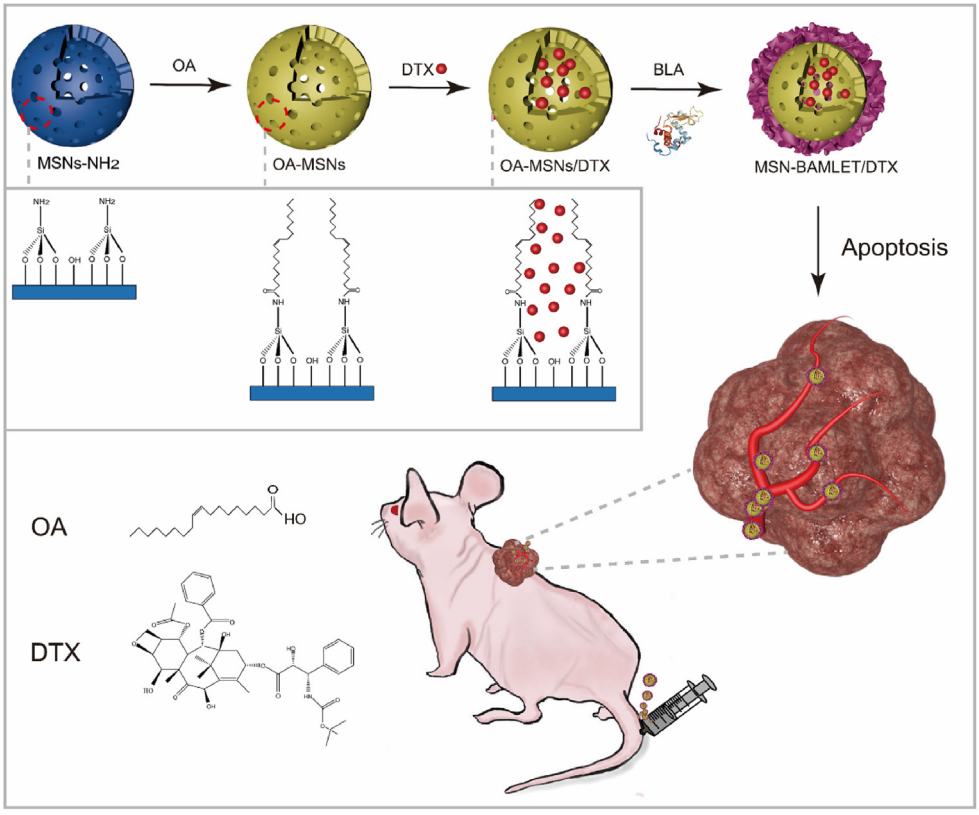

Fig. 1. Schematic diagram of the preparation of DTX loaded MSN-BAMLET. The cartoon diagram of α-lactalbumin was created using Mol* with the PDB ID 1A4V [44]. The formed BAMLET on the silica surface was shown in purple.

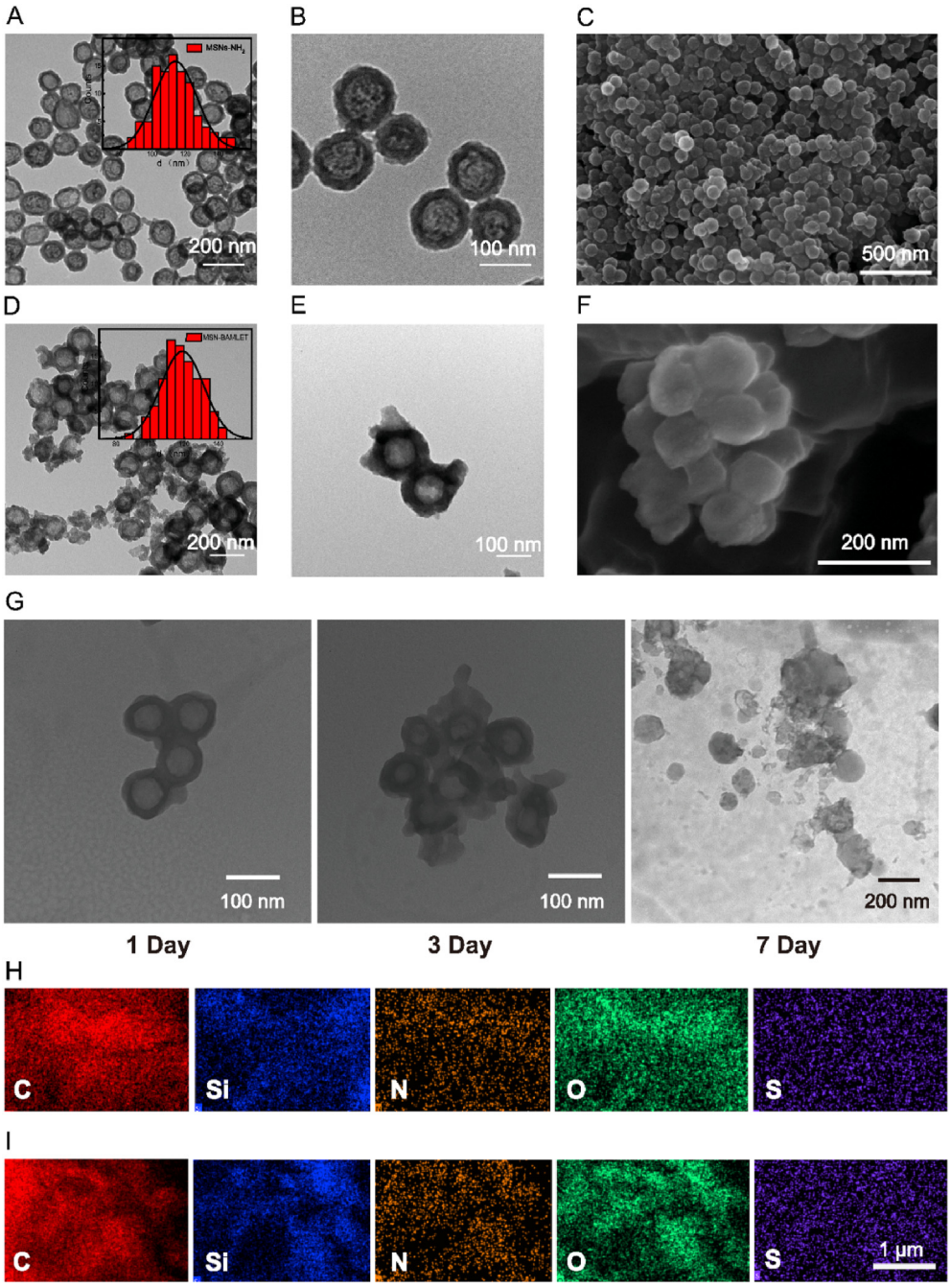

Fig. 2. Morphological features of obtained nanomaterials. TEM, SEM images of MSNs-NH_2 (A, B, C) and MSN-BAMLET (D, E, F). The insert pictures are size distribution of MSNs-NH_2 (A) and MSN-BAMLET (D). (G) Biodegradation behavior of MSN-BAMLET. TEM images were acquired at 1-, 3- and 7-day incubation. Elemental mapping images of OA-MSNs/DTX (H) and MSN-BAMLET/DTX (I). (Scale bar: 1 μm).

average particle size of ~114.03 nm. The surface morphology of OA-MSNs was observed by SEM reflecting a mono-disperse distribution of formed nanomaterials. (Figure S1). As expected, when BLA was conjugated, the average size of MSN-BAMLET was increased to ~119 nm (Fig. 2D, E, F). Furthermore, after 3-day incubation in PBS, irregular aggregates were identified in the sample of MSN-BAMLET (Fig. 2G) reflected by the increased values of hydrodynamic meter suggesting the degradation of nanoparticles (Figure S2A). This observation indicated that the desirable biodegradability of tested nanoparticles in comparison with that of traditional inert organosilica framework [19,45,46].

The surface element distribution of OA-MSNs/DTX (Fig. 2H, Figure S1B) and MSN-BAMLET/DTX (Fig. 2I, Figure S1C) was determined via EDS. From the elemental mapping analysis, the homogeneous elemental distribution of carbon (C), oxygen (O), silicon (Si) and sulfur (S) was observed.

To examine the surface modifications of the formed composite, the spectra of samples by Fourier transformed infrared spectroscopy (FT-IR) was recorded. As shown in Fig. 3A and B, for both OA-MSNs and OA-

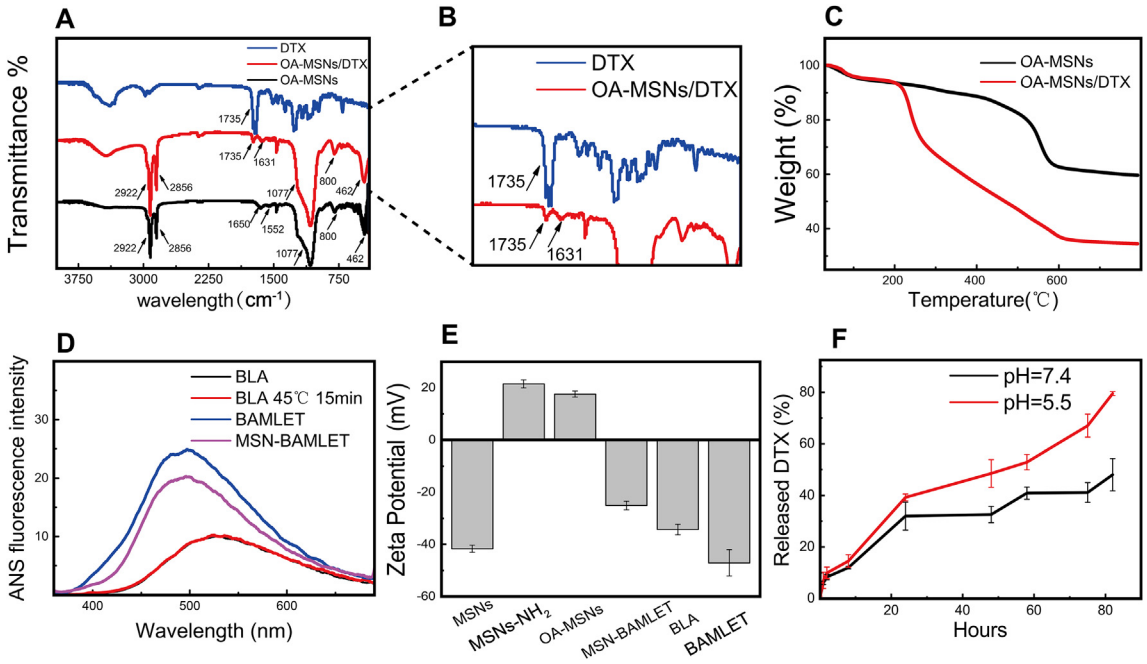

Fig. 3. (A) FT-IR spectra of silica composites and (B) enlarged region to show the characteristic peaks of samples. (C) TGA curves of OA-MSNs and OA-MSNs/DTX. (D) ANS spectra of BLA, BLA after 15 min heat shock at 45 °C, BAMLET and MSN-BAMLET reflecting surface hydrophobicity. (E) Zeta potential of nanoparticles. (F) DTX release profiles of MSN-BAMLET/DTX at pH 5.5 and 7.4.

MSNs/DTX, the broad peak at 1077 cm^{-1} was corresponding to the Si–O asymmetric stretching and the peaks at 800, 462 cm^{-1} can be ascribed to the Si–O symmetric stretching and Si–O–Si anti-symmetric stretching vibrations, respectively. Appearance of two peaks at about 2922 and 2856 cm^{-1} were the stretching vibrations of C–H presented on the surface of amino-functionalized MSNs. Compared to that of the MSNs-NH_2 (Figure S2B), FT-IR spectrum of OA-MSNs showed a new peak at 1552 cm^{-1} due to the formation of amide band supporting the successful grafting of OA on the surface of materials. The FT-IR spectrum of OA-MSNs/DTX was also recorded in comparison with that of OA-MSNs and DTX. The peaks of OA-MSNs at 1650 cm^{-1} corresponding to the bending vibration of silanol-OH shifted to lower positions at 1631 cm^{-1} in OA-MSNs/DTX [47], which may be due to the interaction between DTX and OA-MSNs. The vibration of C–H was getting more pronounced after the loading of DTX at 2922 and 2856 cm^{-1}. In addition, the appearance of a new peak at 1735 cm^{-1} from C═O stretching validated the presence of DTX in the mesopore [48]. TGA was employed to further evaluate the loading of DTX. As shown in Fig. 3C, the initial weight loss at about 100 °C is attributed to the volatilization of absorbed water. The thermal degradation curve of OA-MSNs involved the main weight loss in the temperature range of 200–600 °C due to the decomposition of aminopropyl groups. Moreover, the weight loss at 200–450 °C may result from the degradation of OA molecules [49]. The thermal curve of OA-MSNs/DTX showed more weight loss at the temperature of 800 °C than that of OA-MSNs, which is mainly due to the degradation of DTX. The variation in drug loading efficiency measured by HPLC and TGA is accounting for the difference in method.

Based on the analysis of SDS-PAGE, the band at ~14.0 kDa of MSN-BAMLET with the molecular weight of protein was similar with that of α-lactalbumin (Figure S3). ANS is a molecular probe with high fluorescence intensity in the hydrophobic environment [50]. ANS spectra of BAMLET and MSN-BAMLET with a hypochromic shift and increased intensity reflected a higher surface hydrophobicity compared with that of native BLA (Fig. 3D). The spectra of BLA with heat shock at 45 °C has no difference with that of native BLA demonstrating the superior thermal stability of the protein, which shows that OA is a key factor in the stable conformation of BAMLET [51,52]. Moreover, the recorded Zeta surface potential of formed nanocomposites also revealed the successful chemical modification of MSNs and protein conjugation, in which the MSN-BAMLET showed a negative −25.1 mV as compared with +17.6 mV of OA-MSNs (Fig. 3E).

DTX is one of the most effective aromatic anticancer drugs while its poor water solubility may restrict its clinical applications [10]. Through the loading of drug molecules in the mesopores in the dichloromethane followed by the dispersion of obtained nanocomposites in the aqueous solution, DTX was successfully encapsulated with enhanced water solubility in the nanocarriers. To quantify the loading capacity, the concentration of DTX was measured by HPLC system using a C18 column. The analysis result indicated that the drug loading efficiency of DTX was 73.2% in OA-MSNs and 43.5% in MSNs-NH_2, respectively. The supernatants during the loading process were measured directly by HPLC, which indicated the higher drug loading capacity of OA-MSNs than that of MSNs-NH_2. Such high drug loading capacity of the nanocomposite can be explained by the lipophilic surface of OA grafted MSNs facilitating the adsorption of hydrophobic molecules [53,54]. Moreover, efficient DTX loading in the OA-MSNs was also attributed to the formation of hydrogen bonds between their functional groups [55]. After the protein conjugation on OA-MSNs, the drug loading efficiency of MSN-BAMLET was found to be 38.9%.

To further analyze the release of DTX *in vitro,* MSN-BAMLET/DTX was immersed in PBS at 37 °C. A pH-dependent sustained drug release behaviors was observed as shown in Fig. 3F. In total, 48.04% of total loaded DTX was observed to release after 82 h at pH 7.4 which is much lower than the 79.50% DTX release at pH 5.5 within the same incubation time. We reasoned that an acidic environment increased the protonation of functional groups of the nanocarrier and influenced the hydrogen bonding as well as polar interactions between DTX and the OA-MSNs. Moreover, decreased pH value may weaken the electrostatic attraction between OA-MSNs and BLA as a result of the less negative charge of proteins, which will accelerate the release of supported drugs [56]. The calibration curve of DTX obtained by HPLC system was shown in Figure S4.

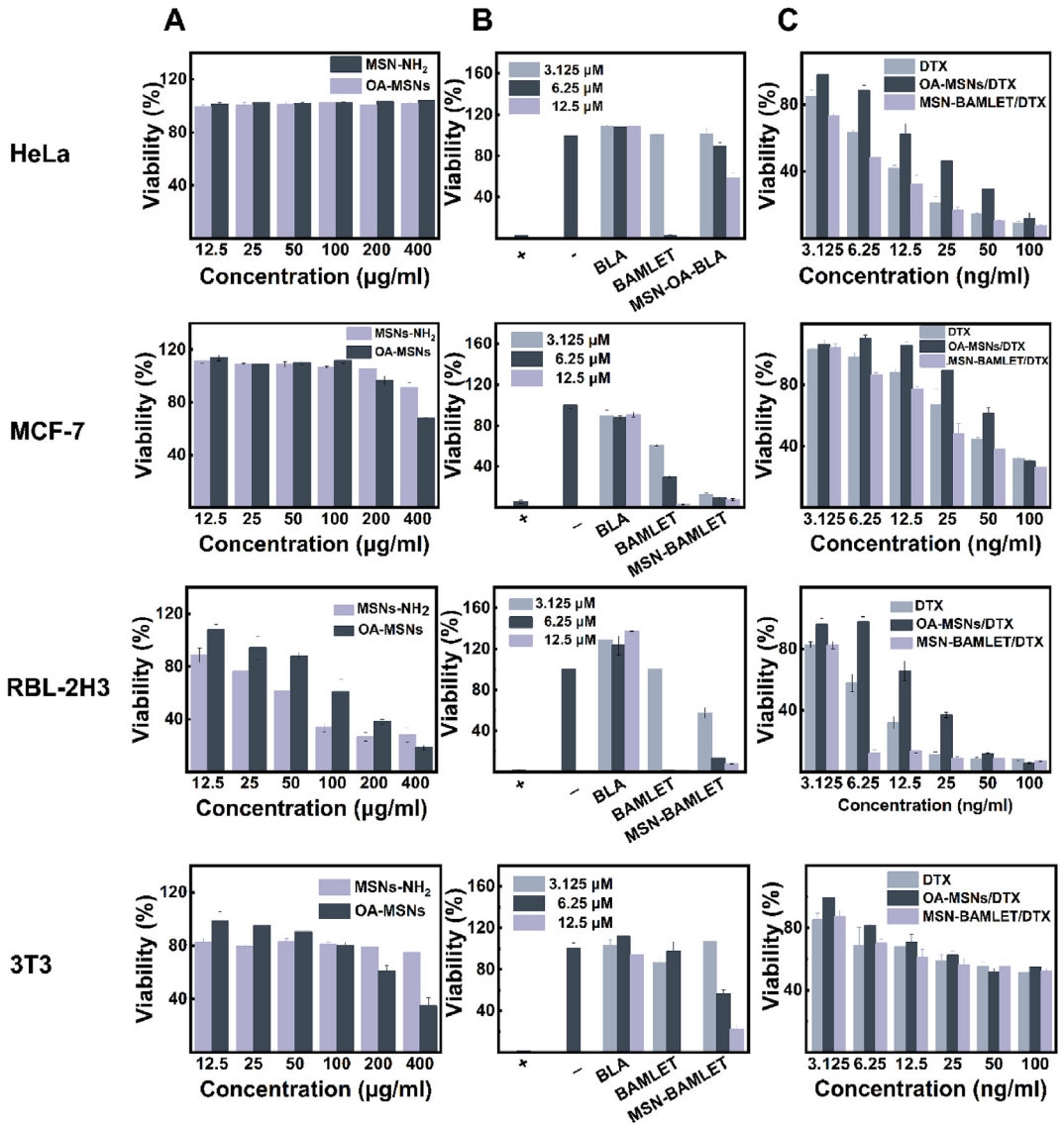

Fig. 4. Relative viability of cells after 72 h of treatment with different concentrations of (A) nude nanoparticles, (B) protein coated MSNs and (C) DTX loaded nanocarriers.

Despite the high drug loading capacity of these nanoparticles, the presence of oleic acid on the surface of OA-MSNs induced the poor water solubility. The dispersibility of nanomaterials was significantly improved when the bovine α-lactalbumin was coated onto the surface of OA-MSNs. The presence of protein in the obtained nanocarriers were quantitated by the bicinchoninic acid (BCA) assay, which showed that the protein ratio of MSN-BAMLET and BAMLET is 23.41% and 44.26% ($m_{protein}/m_{nanoparticle}$ *100), respectively.

The cytotoxicity study of nanoparticles was examined in four different cell lines: cervical tumor cells (HeLa) and breast cancer cells (MCF-7) were chosen representing the highly malignant and invasive cancer types. In addition, the rat basophil leukemia cells (RBL-2H3) were used to testify the broad-spectrum anticancer activity of the sample. The murine embryonic fibroblasts (3T3) were included to test the selectivity of formed nanoparticles towards normal cells. Four different cell lines co-incubated with MSNs-NH_2 and OA-MSNs without drugs showed no observable cytotoxicity at a concentration up to 100 μg/ml except RBL-2H3 cells using a range of concentrations (12.5–400 μg/ml) (Fig. 4A). By comparison, once the BLA was coated onto the OA-MSNs to form MSN-BAMLET, the obvious cytotoxicity was presented to all cancer cell lines at the same protein concentrations of 3.125–12.5 μM (Fig. 4B). Therefore, the identified cytotoxicity of MSN-BAMLET against cancer cells supported that the prepared OA grafted MSNs preserved the tumoricidal effect of BAMLET-like complex. Moreover, BAMLET and MSN-BAMLET showed selective toxicity presenting higher cell viability to fully differentiated cells (3T3) than cancer cells [57]. However, BAMLET in high concentration (12.5 μM) still owned effective cytotoxicity to mature differentiated cells (Fig. 4B). To study the cytotoxic effect of produced DTX loaded nanocomposites, the morphology of the HeLa cells was observed using an optical microscope. As shown in Figure S5, in contrast to normal star shaped HeLa cell, cells treated with MSN-BAMLET/DTX for 72 h transformed into the round shape detached from the bottom of plates. Next, to further study the function of BLA, cell viability of obtained samples was conducted using CCK-8 assay. As shown in Fig. 4C, DTX-loaded nanocarriers and DTX alone were incubated with cancer cells for 72 h at the drug concentrations of 3.125–100 ng/ml. The poor solubility of DTX in cell medium induced relatively low cytotoxicity when compared to that of MSN-BAMLET/DTX. Notably, BLA

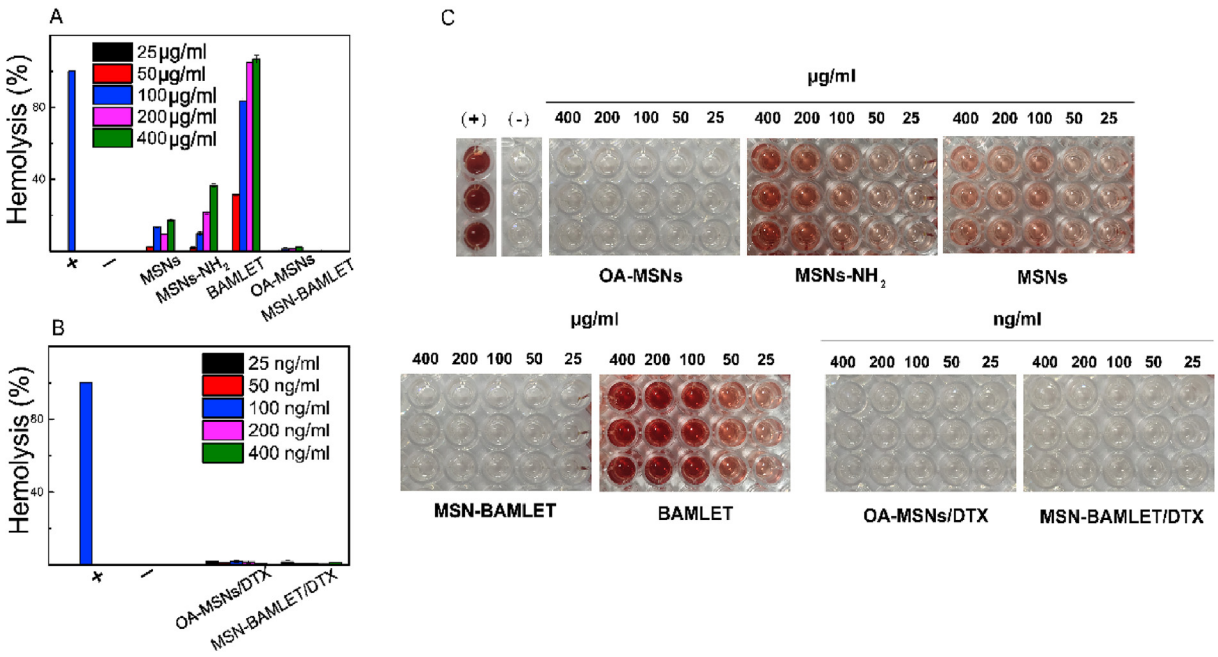

Fig. 5. (A) Hemolysis assay of different nanomaterials including MSNs, MSNs-NH_2, BAMLET, OA-MSNs, MSN-BAMLET, and (B) OA-MSNs/DTX in comparison with MSN-BAMLET/DTX. (C) Hemolytic assay images of samples.

coated OA-MSNs as drug nanocarrier possessed improved anticancer cells effect compared with that of OA-MSNs/DTX possible due to the conjugation of BLA with surface immobilized OA endowing the siliceous composite membrane-disruptive function reminiscent of BAMLET complex [58]. Therefore, the formed BAMLET on the mesoporous silica surface is pivotal for the anticancer efficacy of the constructed system. However, MSN-BAMLET/DTX killed cancer cells more effectively than nontransformed cells (3T3).

While BAMLET showing selective cytotoxicity, it demonstrated strong hemolytic activity [34] that may be not desirable for the practical uses. The underlying mechanism is still under investigation but previous studies have indicated that free oleic acid may be the key role to induce erythrocyte hemolysis as the formed BAMLET or the bound OA actively interacted with the cell surface molecules [59]. Due to the non-toxic nature and enlarged surface area of the siliceous mesopore, we attempted to graft OA onto the surface of MSNs to improve the biocompatibility of the composite materials. As expected, during the incubation of 24 h, both the prepared MSN-BAMLET and DTX loaded nanoparticles exhibited strong hemocompatibility until a concentration as high as 400 μg/ml and 400 ng/ml, respectively (Fig. 5A and B). By comparison, MSNs and MSNs-NH_2 induced observable hemolysis before the oleic acid modification. The relevant Hemolytic assay images of samples were shown in Fig. 5C.

The cell death is usually associated with the appearance of cell lysis and the release of cellular contents [60]. To evaluate the anticancer effect of synthesized nanocomposites, the concentration of extracellular release of nucleic acid was measured by incubating HeLa cells with the composites and free drugs at different [DTX] of 3.125, 6.25, 12.5, 25 and 50 ng/ml, respectively. As expected, MSN-BAMLET/DTX showed stronger cytotoxic effect toward tumor cells than that of OA-MSNs/DTX and DTX, which was consistent with the cytotoxicity observations (Figure S6).

Furthermore, we measured the cellular uptake of produced nanocomposite by the use of FITC-labeled MSN-BAMLET/DTX. As shown in Fig. 6A, the BLA protein shells in the composite was successfully labeled with the dye of FITC of green fluorescence (Figure S8). With the increased time of incubation, HeLa cells treated with MSN-BAMLET/DTX showed improved fluorescence signals of FITC from the recorded CLSM images. At the time point of 24 h incubation, a large majority of incubated cells were dead upon more cellular uptake of MSN-BAMLET/DTX.

MSN-BAMLET/DTX induced mitochondrial dysfunction, which is the symbol of apoptosis, resulting in mitochondrial membrane depolarization. Mitochondrial membrane potential ($\Delta\Psi m$), is an important parameter of mitochondrial function and has been used as an indicator of cell health. To study the variation of $\Delta\Psi m$, lipophilic cationic probe of JC-1 was used. In healthy cells with high $\Delta\Psi m$, JC-1 forms complexes known as J-aggregates with red fluorescence. While in cells with low $\Delta\Psi m$, JC-1 remains as the monomeric form with green fluorescence. As shown in Fig. 6B, HeLa cells treated with drug loaded nanomaterials presented a significant shift of red fluorescence (top left gate) into green fluorescence (bottom right gate) causing mitochondrial depolarization (bottom left). Moreover, MSN-BAMLET led to mitochondrial dysfunction as same as BAMLET which indicated the successful encapsulation of BLA onto the surface of OA-MSNs. To look further into the anticancer mechanism of nanocomplexes, the cytotoxic effect of different nanocomposites including OA-MSNs/DTX, MSN-BAMLET/DTX and free DTX on the HeLa cells after 72-h incubation was studied by the flow cytometry. As shown in Fig. 6C, after the positive staining of cells with Annexin V-FITC and propidium iodide (PI), all treated samples displayed the outer-membrane *trans*-situation of phosphatidylserine and the damage of membrane-integrity. Consequently, MSN-BAMLET/DTX showed significantly higher percentage of cells in both early and late apoptotic/necrotic cell populations at ~88.3% than that of OA-MSNs/DTX (62.9%) and DTX (76.14%) at the same drug concentration of 50 ng/ml.

The invasion of tumor into normal tissues induced poor prognosis [61]. To study the inhibitory effect of the composite on the migration of tested cancel cells, the wound-healing test was conducted by measuring the scratch area of treated cells at 0, 24, 48 and 72 h on an inverted fluorescence microscope (Fig. 7A). It was observed that the cells moved

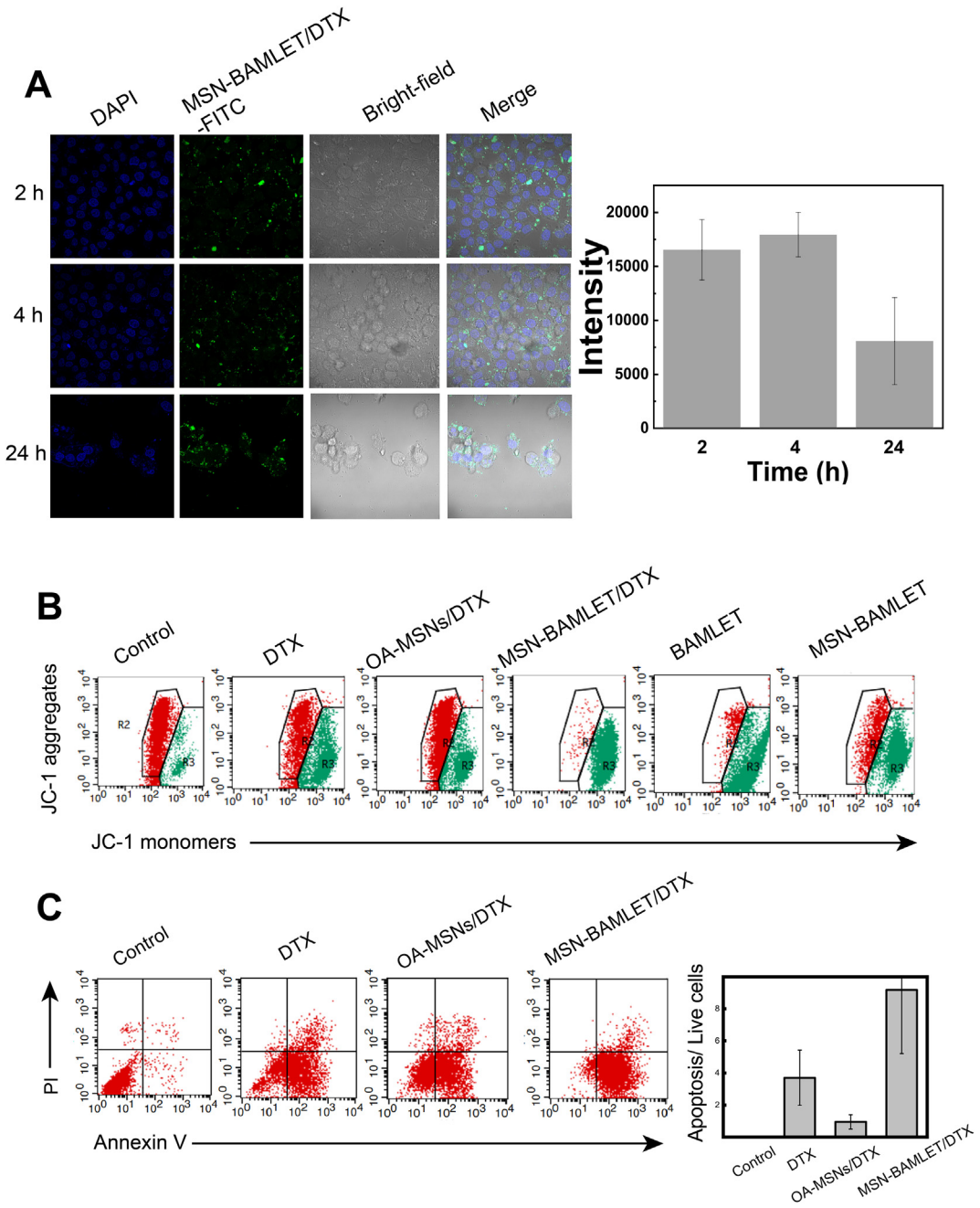

Fig. 6. (A)CLSM images of HeLa cells incubated with MSN-BAMLET/DTX. Flow cytometry analysis of (B) mitochondrial membrane potentials using lipophilic cationic JC-1. (C) the apoptosis/necrosis of the tumor cells.

slowly to the scratched area both in the MSN-BAMLET/DTX and OA-MSNs/DTX group after 72 h incubation. The resulting migration curves showed apparently the inhibitory efficiency of MSN-BAMLET/DTX against the cell migration (Fig. 7B). By comparison, the cells treated with DTX migrated to the blank area in a fast manner. We subsequently created a zebrafish tumor model in which HeLa cells tagged with DiI dye were injected into the yolk sac of embryos. Tumor cells treated with PBS (Fig. 7C) and DTX (Fig. 7F) were observed to move away from the primary sites on day 2 after implantation, but almost all tumor cells in the treatment group of OA-MSNs/DTX (Fig. 7D) and MSN-BAMLET/DTX (Fig. 7E) remained at the injection site. Meanwhile, we found that the group immersed in MSN-BAMLE/DTX solution shows the weakest fluorescence intensity in yolk space (Figure S7).

Protein corona is an active biomolecule layer that forms on the surface of nanoparticles (NPs) after exposure to biological fluids and may have a substantial impact on the nanoparticles' interactions with living systems [62]. It has been suggested that the protein corona determines the *in vivo* efficiency of nanomedicine after intravenously administration [63]. The physicochemical features of nanoplatforms, such as material, size, shape, surface modification and charge, NPs

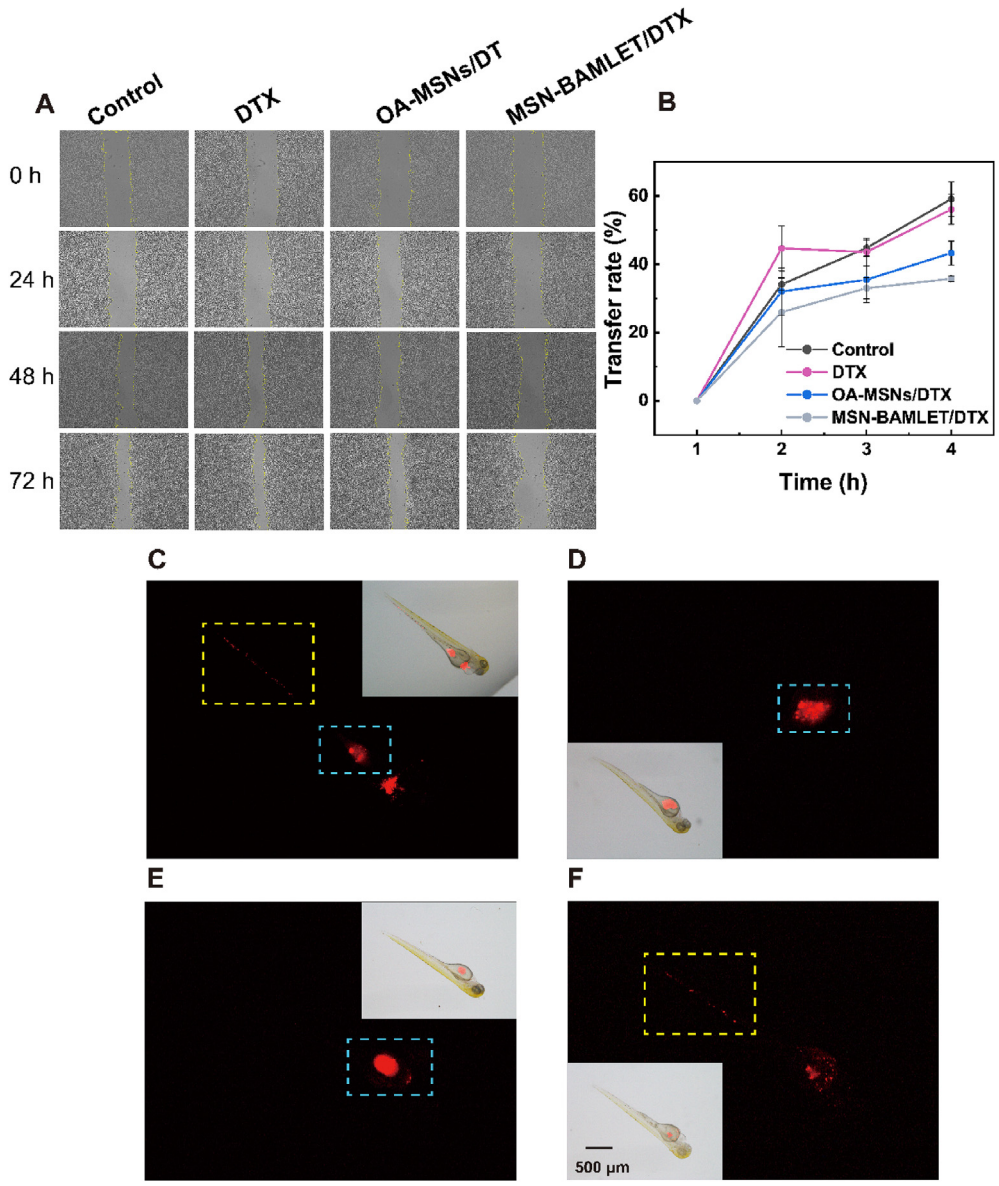

Fig. 7. (A) Wound-healing assay of HeLa cells treated with DTX, OA-MSNs/DTX, and MSN-BAMLET/DTX. (B) The quantification result of the wound-healing assay. Images of (C) PBS, (D) OA-MSNs/DTX, (E) MSN-BAMLET/DTX, (F) DTX treated zebrafish after injection of HeLa cell line into embryos. Cell injection and migration sites are represented by blue and yellow circles, respectively.

hydrophilicity/hydrophobicity, and the composition of biological fluid, all influence the components of protein corona [64]. Protein corona adsorbed on to the MSNs, MSNs-NH_2, OA-MSNs and MSN-BAMLET with or without DTX was characterized by the SDS-PAGE analysis. The gel staining by Coomassie Brilliant Blue revealed the complicated band patterns of the adsorbed proteins. The control lane was 10% serum incubating without any NPs. In comparison with MSNs-NH_2, the overall amount of protein was increased on the surface of OA-MSNs accounting for the hydrophobic surface induced by oleic acid modification, which resulted in the higher protein adsorption capacity of the nanomaterial [64]. Notably, both MSN-BAMLET and MSN-BAMLET/DTX showed similar band profiles with lowest amount and abundance of protein indicating their promising potential to reduce the interaction with plasma proteins. Note that immunoglobulin G (IgG), the most abundant type of immunoglobulin in the blood acting to remove antigen in the blood, possessed a molecular weight of approximately 150 kDa [65]. In the gel, there were virtually no observable bands corresponding to the protein molecular weight of 100–250 kDa indicating that the removal of MSN-BAMLET/DTX by the immune system could be reduced to a great extent. (Figure S9).

The clinical uses of BAMLET were limited especially in endovascular treatment for the reason that the serum in blood could weaken the tumoricidal activity (Table S1). By comparison, upon grafting oleic acid onto the surface of MSNs, we found that MSN-BAMLET exhibited more potent anticancer activity than BAMLET in medium with 20% serum. We then performed an animal study to further investigate the therapeutic efficacy of drug loading MSN-BAMLET. Fig. 8A showed the design of *in vivo* cancer therapy in which we challenged mice with different

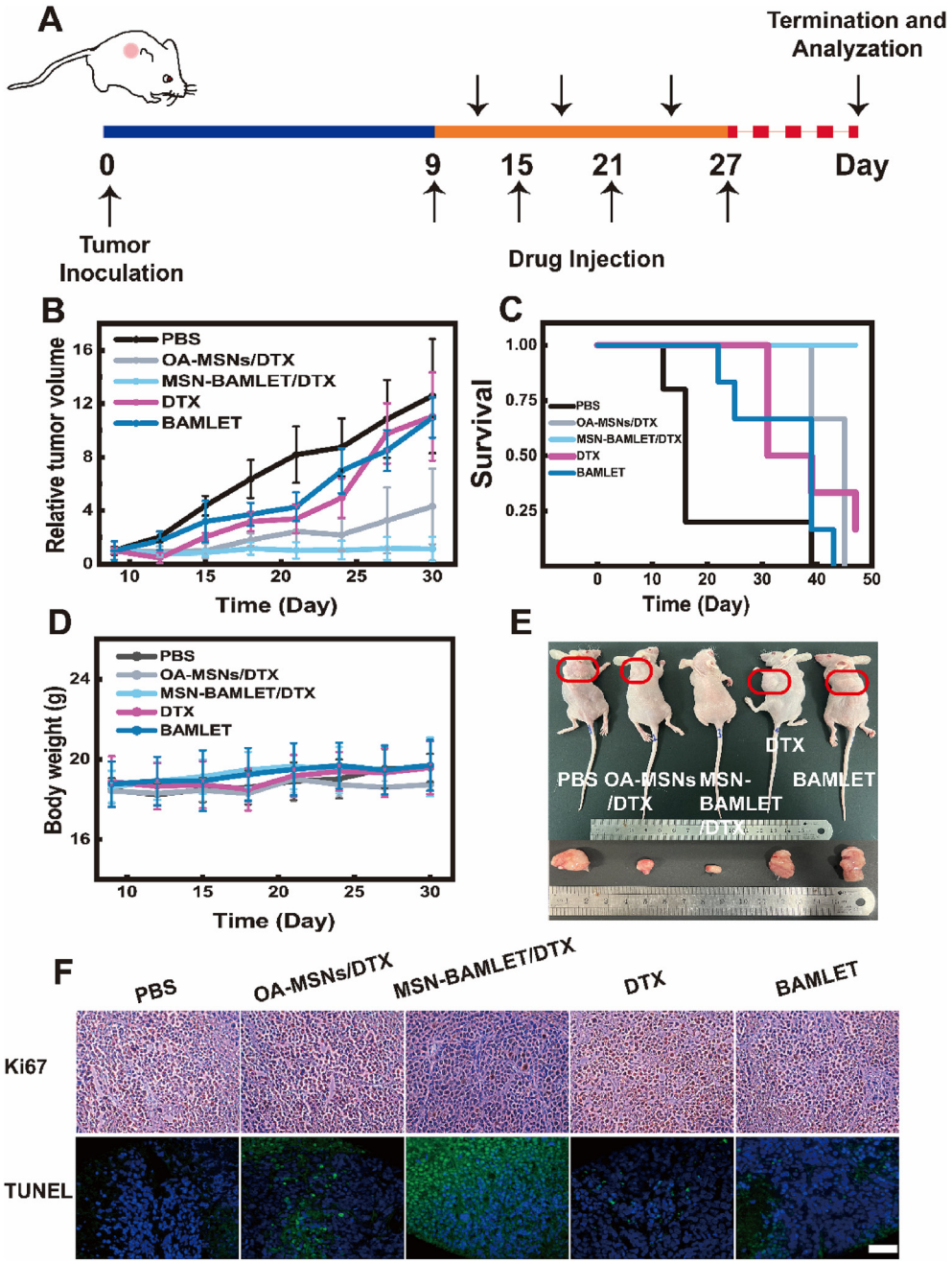

Fig. 8. (A) Protocol of anticancer therapy. (B) Tumor volume of cancer bearing mice after different treatment. (C) Survival curves of mice. (D) Body weight changes of different groups. (E) Photograph of dissected solid tumor. (F) histological analysis of tumor section (scale bar: 50 μm).

treatments on day 9, 12, 15, 18, 21, 24, 27 and measured the body weights and tumor volumes. As shown in Fig. 8B, the result indicated that the MSN-BAMLET/DTX significantly inhibited tumor development than the OA-MSNs/DTX, DTX and BAMLET. To further test the treatment effect, we conducted a long term close observation of mice after various treatments and found that the survival time after the MSN-BAMLET/DTX injection was prominently extended (Fig. 8C). Consistent experimental results were also reflected in the recorded tumor images (Fig. 8E) of the sacrificed mice. It was found that the body weight of each groups did not show an obvious difference and the mice did not present abnormal during the treatment [66,67] (Fig. 8D). To detect cell apoptosis, TUNEL assay was performed. It could be observed that the tumor cells from MSN-BAMLET/DTX treated mice showed the most significant TUNEL fluorescence signal of all treatment groups. Moreover, MSN-BAMLET/DTX inhibited the cell proliferation, which was also validated by Ki67 staining observations (Fig. 8F). By contrast, no observable damages in nomal organs testified the biocompatibility of obtained nanoparticles *in vivo* (Fig. 9). Furthermore, the outcomes of blood biochemistry was shown in Figure S10, which indicated the promosing therapeutic potential of constructed MSN-BAMLET/DTX as biosafe drug delivery system.

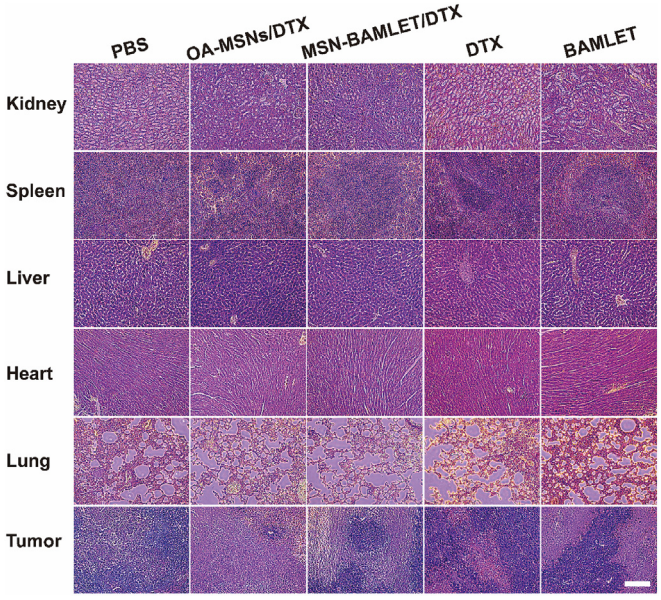

Fig. 9. Histopathological evaluation by hematoxylin-eosin (H&E) staining for different organs and tumors harvested after different treatments (scale bar: 200 μm).

4. Conclusions

The widely known anticancer agent of BAMLET preserved the broad-spectrum tumoricidal effect and selective cytotoxicity. The lipoprotein complex was formed by the bovine α-lactalbumin of partially unfolded conformation that was stabilized by the complexation with oleic acids, which usually involved a labor-intensive process that remains an obstacle for the scale-up manufacture. Additionally, the pronounced hemolytic activity of BAMLET was identified in previous studies may limit its clinical application. In this study, we developed a mesoporous silica-based therapeutic nanoplatform resembling the BAMLET-like complex by the conjugation of surface grafted OA with BLA. Taking advantage of nontoxic MSNs with large surface area, the supported MSN-BAMLET complex exhibited desirable high biocompatibility. Moreover, the formed MSN-BAMLET complex with oleic acid modifications was efficient to load hydrophobic drug of DTX. It was observed that at the same concentration of DTX, the produced MSN-BAMLET exhibited more pronounced cytotoxic effect against cancer cells than that of OA-MSNs due to the more cellular uptake and stronger inhibitory effect on the cell migrations of the BLA conjugated nanocomposite. Significantly, α-lactalbumin coated MSNs exhibited lowest amount and abundance of protein absorption which may reduce its interaction with plasma proteins and realize long circulation. We also verified that the BAMLET encapsulated MSNs can significantly enhance the antitumor efficiency *in vivo* than single drug treatment. Therefore, the produced MSN-BAMLET of high biocompatibility as a manipulable nanoplatform holds enormous potentials for the therapeutic purposes. Recently, stimuli-responsive drug release systems such as pH and NIR (near-infrared)-triggered systems were developed [68–70]. Therefore, in a long run, the further synergistic therapeutic strategies based on the use of MSN-BAMLET are expected to improve the efficiency of tumor ablation.

Authors' contributions

WP, LC and LZ performed the experiment. WP analyzed the data. WP, XG and CW performed the zebrafish experiment. JZ performed the protein experiment. PZ performed the silica material experiment. HJ, SW and JC supervised experiment. WP drafted the manuscript. JC conceived and designed the experiment and revised the manuscript. All authors read and approved the final manuscript.

Credit author statement

Wei Pei: Methodology, Investigation, Writing – original draft. Ling Cai, Xing Gong, Li Zhang, Jiarong Zhang, Ping Zhu, Chao Wang: Methodology, Investigation. Huijun Jiang, Shoulin Wang: Methodology, Supervision. Jin Chen: Conceptualization, Supervision, Writing – review & editing.

Declaration of competing interest

The authors declare that they have no known competing financial interests or personal relationships that could have appeared to influence the work reported in this paper.

Acknowledgements

We thank the financial support of National Natural Science Foundation of China (U1703118), Natural Science Foundation of Jiangsu Higher Education Institutions of China (No. 19KJA310003), Natural Science Foundation of Jiangsu Province (No. BK20181364), a project funded by the Priority Academic Program Development of Jiangsu Higher Education Institutions (PAPD), and the Open Project of Jiangsu Biobank of Clinical Resources, No. 13.

Appendix A. Supplementary data

Supplementary data to this article can be found online at https://doi.org/10.1016/j.mtbio.2022.100272.

References

[1] Y.Q. Liu, X.L. Wang, D.H. He, Y.X. Cheng, Protection against chemotherapy- and radiotherapy-induced side effects: a review based on the mechanisms and therapeutic opportunities of phytochemicals, Phytomedicine 80 (2021) 153402, https://doi.org/10.1016/j.phymed.2020.153402.
[2] Z.W. Ma, N. Wang, H.B. He, X. Tang, Pharmaceutical strategies of improving oral systemic bioavailability of curcumin for clinical application, J. Contr. Release 316 (2019) 359–380, https://doi.org/10.1016/j.jconrel.2019.10.053.
[3] K.D. Miller, L. Nogueira, A.B. Mariotto, J.H. Rowland, K.R. Yabroff, C.M. Alfano, A. Jemal, J.L. Kramer, R.L. Siegel, Cancer treatment and survivorship statistics, 2019, Ca-a Cancer Journal for Clinicians 69 (2019) 363–385, https://doi.org/10.3322/caac.21565.
[4] F. Chast, Obituary: pierre potier (1934-2006), Nature 440 (2006) 291.
[5] J.E. Cortes, R. Pazdur, Docetaxel, J. Clin. Oncol. 13 (1995) 2643–2655.
[6] Y. Hu, M. Ran, B. Wang, Y. Lin, Y. Cheng, S. Zheng, Co-delivery of docetaxel and curcumin via nanomicelles for enhancing anti-ovarian cancer treatment, Int. J. Nanomed. 15 (2020) 9703–9715, https://doi.org/10.2147/IJN.S274083.
[7] C. Yan, L. Gao, X. Qiu, C. Deng, Schisandrin B synergizes docetaxel-induced restriction of growth and invasion of cervical cancer cells and, Ann. Transl. Med. 8 (2020) 1157, https://doi.org/10.21037/atm-20-6109.
[8] M. Hecht, A.O. Gostian, M. Eckstein, S. Rutzner, J. von der Grün, T. Illmer, M.G. Hautmann, G. Klautke, S. Laban, T. Brunner, A. Hinke, I. Becker, B. Frey, S. Semrau, C.I. Geppert, A. Hartmann, P. Balermpas, W. Budach, U.S. Gaipl, H. Iro, R. Fietkau, Safety and efficacy of single cycle induction treatment with cisplatin/

docetaxel/durvalumab/tremelimumab in locally advanced HNSCC: first results of CheckRad-CD8, J Immunother Cancer 8 (2020), https://doi.org/10.1136/jitc-2020-001378.
[9] O. Arrieta, F. Barrón, L.A. Ramírez-Tirado, Z.L. Zatarain-Barrón, A.F. Cardona, D. Díaz-García, M. Yamamoto Ramos, B. Mota-Vega, A. Carmona, M.P. Peralta Álvarez, Y. Bautista, F. Aldaco, R. Gerson, C. Rolfo, R. Rosell, Efficacy and safety of pembrolizumab plus docetaxel vs docetaxel alone in patients with previously treated advanced non-small cell lung cancer: the PROLUNG phase 2 randomized clinical trial, JAMA Oncol. 6 (2020) 856–864, https://doi.org/10.1001/jamaoncol.2020.0409.
[10] E. Zhang, R. Xing, S. Liu, P. Li, Current advances in development of new docetaxel formulations, Expet Opin. Drug Deliv. 16 (2019) 301–312, https://doi.org/10.1080/17425247.2019.1583644.
[11] D. Bhunia, A. Saha, A. Adak, G. Das, S. Ghosh, A dual functional liposome specifically targets melanoma cells through integrin and ephrin receptors, RSC Adv. 6 (2016) 113487–113491, https://doi.org/10.1039/c6ra23864e.
[12] J. Gao, S. Jiang, X. Zhang, Y. Fu, Z. Liu, Preparation, characterization and in vitro activity of a docetaxel-albumin conjugate, Bioorg. Chem. 83 (2019) 154–160, https://doi.org/10.1016/j.bioorg.2018.10.032.
[13] R.P. Singh, G. Sharma, Sonali, S. Singh, S. Bharti, B.L. Pandey, B. Koch, M.S. Muthu, Chitosan-folate decorated carbon nanotubes for site specific lung cancer delivery, Materials Science & Engineering C-Materials for Biological Applications 77 (2017) 446–458, https://doi.org/10.1016/j.msec.2017.03.225.
[16] Q. Yue, J.L. Li, W. Luo, Y. Zhang, A.A. Elzatahry, X.Q. Wang, C. Wang, W. Li, X.W. Cheng, A. Alghamdi, A.M. Abdullah, Y.H. Deng, D.Y. Zhao, An interface coassembly in biliquid phase: toward core-shell magnetic mesoporous silica microspheres with tunable pore size, J. Am. Chem. Soc. 137 (2015) 13282–13289, https://doi.org/10.1021/jacs.5b05619.
[17] X.G. Liu, F. Zhang, X.X. Jing, M.C. Pan, P. Liu, W. Li, B.W. Zhu, J. Li, H. Chen, L.H. Wang, J.P. Lin, Y. Liu, D.Y. Zhao, H. Yan, C.H. Fan, Complex silica composite nanomaterials templated with DNA origami, Nature 559 (2018) 593–598, https://doi.org/10.1038/s41586-018-0332-7.
[18] X.M. Li, L. Zhou, Y. Wei, A.M. El-Toni, F. Zhang, D.Y. Zhao, Anisotropic growth-induced synthesis of dual-compartment janus mesoporous silica nanoparticles for bimodal triggered drugs delivery, J. Am. Chem. Soc. 136 (2014) 15086–15092, https://doi.org/10.1021/ja508733r.
[19] Z. Li, Y. Yang, H. Wei, X. Shan, X. Wang, M. Ou, Q. Liu, N. Gao, H. Chen, L. Mei, X. Zeng, Charge-reversal biodegradable MSNs for tumor synergetic chemo/photothermal and visualized therapy, J. Contr. Release : Official Journal of the Controlled Release Society 338 (2021) 719–730, https://doi.org/10.1016/j.jconrel.2021.09.005.
[20] Z.G.Y.L.W. Li, Charge-reversal nanomedicines as a smart bullet for deep tumor penetration, Smart Materials in Medicine 3 (2022) 243–253, https://doi.org/10.1016/j.smaim.2022.01.008.
[21] P. Huang, D.Z. Lian, H.L. Ma, N.S. Gao, L.M. Zhao, P. Luan, X.W. Zeng, New advances in gated materials of mesoporous silica for drug controlled release, Chin. Chem. Lett. 32 (2021) 3696–3704, https://doi.org/10.1016/j.cclet.2021.06.034.
[22] A. Barkat, S. Beg, S.K. Panda, K. S Alharbi, M. Rahman, F.J. Ahmed, Functionalized mesoporous silica nanoparticles in anticancer therapeutics, Semin. Cancer Biol. 69 (2021) 365–375, https://doi.org/10.1016/j.semcancer.2019.08.022.
[23] R.R. Castillo, D. Lozano, B. Gonzalez, M. Manzano, I. Izquierdo-Barba, M. Vallet-Regi, Advances in mesoporous silica nanoparticles for targeted stimuli-responsive drug delivery: an update, Expet Opin. Drug Deliv. 16 (2019) 415–439, https://doi.org/10.1080/17425247.2019.1598375.
[24] H. Mekaru, J. Lu, F. Tamanoi, Development of mesoporous silica-based nanoparticles with controlled release capability for cancer therapy, Adv. Drug Deliv. Rev. 95 (2015) 40–49, https://doi.org/10.1016/j.addr.2015.09.009.
[25] A. Håkansson, B. Zhivotovsky, S. Orrenius, H. Sabharwal, C. Svanborg, Apoptosis induced by a human milk protein, Proc. Natl. Acad. Sci. U. S. A. 92 (1995) 8064–8068.
[26] C. Svanborg, H. Agerstam, A. Aronson, R. Bjerkvig, C. Duringer, W. Fischer, L. Gustafsson, O. Hallgren, I. Leijonhuvud, S. Linse, A.K. Mossberg, H. Nilsson, J. Pettersson, M. Svensson, HAMLET kills tumor cells by an apoptosis-like mechanism–cellular, molecular, and therapeutic aspects, Adv. Cancer Res. 88 (2003) 1–29, https://doi.org/10.1016/s0065-230x(03)88302-1.
[27] A. Nadeem, J.C.S. Ho, T.H. Tran, S. Paul, V. Granqvist, N. Despretz, C. Svanborg, Beta-sheet-specific interactions with heat shock proteins define a mechanism of delayed tumor cell death in response to HAMLET, J. Mol. Biol. 431 (2019) 2612–2627, https://doi.org/10.1016/j.jmb.2019.05.007.
[28] E.A. Permyakov, alpha-lactalbumin, amazing calcium-binding protein, Biomolecules 10 (2020), https://doi.org/10.3390/biom10091210.
[29] T.T. Hien, I. Ambite, D. Butler, M.L.Y. Wan, T.H. Tran, U. Hoglund, M. Babjuk, C. Svanborg, Bladder cancer therapy without toxicity-A dose-escalation study of alpha1-oleate, Int. J. Cancer 147 (2020) 2479–2492, https://doi.org/10.1002/ijc.33019.
[30] L. Gustafsson, I. Leijonhufvud, A. Aronsson, A.K. Mossberg, C. Svanborg, Treatment of skin papillomas with topical alpha-lactalbumin-oleic acid, N. Engl. J. Med. 350 (2004) 2663–2672, https://doi.org/10.1056/NEJMoa032454.
[31] M. Puthia, P. Storm, A. Nadeem, S. Hsiung, C. Svanborg, Prevention and treatment of colon cancer by peroral administration of HAMLET (human alpha-lactalbumin made lethal to tumour cells), Gut 63 (2014) 131–142, https://doi.org/10.1136/gutjnl-2012-303715.
[32] A. Brisuda, J.C.S. Ho, P.S. Kandiyal, J.T.Y. Ng, I. Ambite, D.S.C. Butler, J. Háček, M.L.Y. Wan, T.H. Tran, A. Nadeem, T.H. Tran, A. Hastings, P. Storm, D.L. Fortunati, P. Esmaeili, H. Novotna, J. Horňák, Y.G. Mu, K.H. Mok, M. Babjuk, C. Svanborg, Bladder cancer therapy using a conformationally fluid tumoricidal peptide complex, Nat. Commun. 12 (2021) 3427, https://doi.org/10.1038/s41467-021-23748-y.
[33] W. Fischer, L. Gustafsson, A.K. Mossberg, J. Gronli, S. Mork, R. Bjerkvig, C. Svanborg, Human alpha-lactalbumin made lethal to tumor cells (HAMLET) kills human glioblastoma cells in brain xenografts by an apoptosis-like mechanism and prolongs survival, Cancer Res. 64 (2004) 2105–2112, https://doi.org/10.1158/0008-5472.can-03-2661.
[34] S. Mahanta, S. Paul, Stable self-assembly of bovine alpha-lactalbumin exhibits target-specific antiproliferative activity in multiple cancer cells, ACS Appl. Mater. Interfaces 7 (2015) 28177–28187, https://doi.org/10.1021/acsami.5b06076.
[35] P. Zhu, L. Zhou, Y. Song, L. Cai, M. Ji, J. Wang, G. Ruan, J. Chen, Encapsulating insoluble antifungal drugs into oleic acid-modified silica mesocomposites with enhanced fungicidal activity, J. Mater. Chem. B 8 (2020) 4899–4907, https://doi.org/10.1039/d0tb00106f.
[36] F. Tang, L. Li, D. Chen, Mesoporous silica nanoparticles: synthesis, biocompatibility and drug delivery, Adv. Mater. 24 (2012) 1504–1534, https://doi.org/10.1002/adma.201104763.
[37] Q. Peng, S. Zhang, Q. Yang, T. Zhang, X.-Q. Wei, L. Jiang, C.-L. Zhang, Q.-M. Chen, Z.-R. Zhang, Y.-F. Lin, Preformed albumin corona, a protective coating for nanoparticles based drug delivery system, Biomaterials 34 (2013) 8521–8530, https://doi.org/10.1016/j.biomaterials.2013.07.102.
[38] C.R. Brinkmann, S. Thiel, D.E. Otzen, Proteinfatty acid complexes: biochemistry, biophysics and function, FEBS J. 280 (2013) 1733–1749, https://doi.org/10.1111/febs.12204.
[39] B. Fang, M. Zhang, K.S. Ge, H.Z. Xing, F.Z. Ren, alpha-Lactalbumin-oleic acid complex kills tumor cells by inducing excess energy metabolism but inhibiting mRNA expression of the related enzymes, J. Dairy Sci. 101 (2018) 4853–4863, https://doi.org/10.3168/jds.2017-13731.
[40] Y. He, S. Liang, M. Long, H. Xu, Mesoporous silica nanoparticles as potential carriers for enhanced drug solubility of paclitaxel, Mater Sci Eng C Mater Biol Appl 78 (2017) 12–17, https://doi.org/10.1016/j.msec.2017.04.049.
[41] G. Guan, L. Zhang, J. Zhu, H. Wu, W. Li, Q. Sun, Antibacterial properties and mechanism of biopolymer-based films functionalized by CuO/ZnO nanoparticles against Escherichia coli and Staphylococcus aureus, J. Hazard Mater. 402 (2021) 123542, https://doi.org/10.1016/j.jhazmat.2020.123542.
[42] H.-K. Kim, K.R. Bhattarai, R.P. Junjappa, J.H. Ahn, S.H. Pagire, H.J. Yoo, J. Han, D. Lee, K.-W. Kim, H.-R. Kim, H.-J. Chae, TMBIM6/BI-1 contributes to cancer progression through assembly with mTORC2 and AKT activation, Nat. Commun. 11 (2020) 4012, https://doi.org/10.1038/s41467-020-17802-4.
[43] B. Yin, C.K.W. Chan, S. Liu, H. Hong, S.H.D. Wong, L.K.C. Lee, L.W.C. Ho, L. Zhang, K.C.-F. Leung, P.C.-L. Choi, L. Bian, X.Y. Tian, M.N. Chan, C.H.J. Choi, Intrapulmonary cellular-level distribution of inhaled nanoparticles with defined functional groups and its correlations with protein corona and inflammatory response, ACS Nano 13 (2019) 14048–14069, https://doi.org/10.1021/acsnano.9b06424.
[44] D. Sehnal, S. Bittrich, M. Deshpande, R. Svobodova, K. Berka, V. Bazgier, S. Velankar, S.K. Burley, J. Koca, A.S. Rose, Mol* Viewer: modern web app for 3D visualization and analysis of large biomolecular structures, Nucleic Acids Res. 49 (2021) W431–W437, https://doi.org/10.1093/nar/gkab314.
[45] D. Shao, F. Zhang, F. Chen, X. Zheng, H. Hu, C. Yang, Z. Tu, Z. Wang, Z. Chang, J. Lu, T. Li, Y. Zhang, L. Chen, K.W. Leong, W.-F. Dong, Biomimetic diselenide-bridged mesoporous organosilica nanoparticles as an X-ray-responsive biodegradable carrier for chemo-immunotherapy, Adv. Mater. 32 (2020), e2004385, https://doi.org/10.1002/adma.202004385.
[46] L. Wang, M. Huo, Y. Chen, J. Shi, Iron-engineered mesoporous silica nanocatalyst with biodegradable and catalytic framework for tumor-specific therapy, Biomaterials 163 (2018), https://doi.org/10.1016/j.biomaterials.2018.02.018.
[47] H. Chaudhuri, S. Dash, A. Sarkar, SBA-15 functionalised with high loading of amino or carboxylate groups as selective adsorbent for enhanced removal of toxic dyes from aqueous solution, New J. Chem. 40 (2016) 3622–3634, https://doi.org/10.1039/c5nj02816g.
[48] M.A. Mahmood, A. Madni, M. Rehman, M.A. Rahim, A. Jabar, Ionically cross-linked chitosan nanoparticles for sustained delivery of docetaxel: fabrication, post-formulation and acute oral toxicity evaluation, Int. J. Nanomed. 14 (2019) 10035–10046, https://doi.org/10.2147/IJN.S232350.
[49] A. Pourjavadi, S.S. Amin, S.H. Hosseini, Delivery of hydrophobic anticancer drugs by hydrophobically modified alginate based magnetic nanocarrier, Ind. Eng. Chem. Res. 57 (2018) 822–832, https://doi.org/10.1021/acs.iecr.7b04050.
[50] C. Ota, S.-I. Tanaka, K. Takano, Revisiting the rate-limiting step of the ANS-protein binding at the protein surface and inside the hydrophobic cavity, Molecules 26 (2021), https://doi.org/10.3390/molecules26020420.

[51] M. Svensson, J. Fast, A.K. Mossberg, C. Duringer, L. Gustafsson, O. Hallgren, C.L. Brooks, L. Berliner, S. Linse, C. Svanborg, Alpha-lactalbumin unfolding is not sufficient to cause apoptosis, but is required for the conversion to HAMLET (human alpha-lactalbumin made lethal to tumor cells), Protein Sci. 12 (2003) 2794–2804, https://doi.org/10.1110/ps.0231003.
[52] J. Fast, A.K. Mossberg, C. Svanborg, S. Linse, Stability of HAMLET–a kinetically trapped alpha-lactalbumin oleic acid complex, Protein Sci. 14 (2005) 329–340, https://doi.org/10.1110/ps.04982905.
[53] T.G. Meikle, C.J. Drummond, C.E. Conn, Microfluidic synthesis of rifampicin loaded PLGA nanoparticles and the effect of formulation on their physical and antibacterial properties, Aust. J. Chem. 73 (2020) 151–157, https://doi.org/10.1071/ch19359.
[54] N.A. Azeez, M. Saravanan, N.R.K. Chandar, M.K. Vishaal, V.S. Deepa, Enhancing the aspirin loading and release efficiency of silver oxide nanoparticles using oleic acid-based bio-surfactant fromEnteromorpha intestinalis, Appl. Organomet. Chem. 34 (2020), https://doi.org/10.1002/aoc.5934.
[55] F. Nasrollahi, J. Varshosaz, A.A. Khodadadi, S. Lim, A. Jahanian-Najafabadi, Targeted delivery of docetaxel by use of transferrin/poly(allylamine hydrochloride)-functionalized graphene oxide nanocarrier, ACS Appl. Mater. Interfaces 8 (2016) 13282–13293, https://doi.org/10.1021/acsami.6b02790.
[56] L. Li, W. Sun, L. Li, Y. Liu, L. Wu, F. Wang, Z. Zhou, Z. Zhang, Y. Huang, A pH-responsive sequential-disassembly nanohybrid for mitochondrial targeting, Nanoscale 9 (2017) 314–325, https://doi.org/10.1039/c6nr07004c.
[57] P. Rammer, L. Groth-Pedersen, T. Kirkegaard, M. Daugaard, A. Rytter, P. Szyniarowski, M. Hoyer-Hansen, L.K. Povlsen, J. Nylandsted, J.E. Larsen, M. Jaattela, BAMLET activates a lysosomal cell death program in cancer cells, Mol. Cancer Therapeut. 9 (2010) 24–32, https://doi.org/10.1158/1535-7163.MCT-09-0559.
[58] H.Z. Wen, O. Stromland, O. Halskau, alpha-Lactalbumin:Oleic acid complex spontaneously delivers oleic acid to artificial and erythrocyte membranes, J. Mol. Biol. 427 (2015) 3177–3187, https://doi.org/10.1016/j.jmb.2015.08.009.
[59] M. Hoque, S. Dave, P. Gupta, M. Saleemuddin, Oleic acid may be the key contributor in the BAMLET-induced erythrocyte hemolysis and tumoricidal action, PLoS One 8 (2013), e68390, https://doi.org/10.1371/journal.pone.0068390.
[60] M.S. D'Arcy, Cell death: a review of the major forms of apoptosis, necrosis and autophagy, Cell Biol. Int. 43 (2019) 582–592, https://doi.org/10.1002/cbin.11137.
[61] B. Fang, M. Zhang, H. Wu, X. Fan, F. Ren, Internalization properties of the anti-tumor alpha-lactalbumin-oleic acid complex, Int. J. Biol. Macromol. 96 (2017) 44–51, https://doi.org/10.1016/j.ijbiomac.2016.12.031.
[62] J.Y. Park, S.J. Park, J.Y. Park, S.H. Kim, S. Kwon, Y. Jung, D. Khang, Unfolded protein corona surrounding nanotubes influence the innate and adaptive immune system, Adv. Sci. 8 (2021) 14, https://doi.org/10.1002/advs.202004979.
[63] Y. Liu, J.Q. Wang, Q.Q. Xiong, D. Hornburg, W. Tao, O.C. Farokhzad, Nano-Bio interactions in cancer: from therapeutics delivery to early detection, Accounts Chem. Res. 54 (2021) 291–301, https://doi.org/10.1021/acs.accounts.0c00413.
[64] M. Neagu, Z. Piperigkou, K. Karamanou, A.B. Engin, A.O. Docea, C. Constantin, C. Negrei, D. Nikitovic, A. Tsatsakis, Protein bio-corona: critical issue in immune nanotoxicology, Arch. Toxicol. 91 (2017) 1031–1048, https://doi.org/10.1007/s00204-016-1797-5.
[65] L.C. Fonseca, M.M. de Araujo, A.C.M. de Moraes, D.S. da Silva, A.G. Ferreira, L.S. Franqui, D.S.T. Martinez, O.L. Alves, Nanocomposites based on graphene oxide and mesoporous silica nanoparticles: preparation, characterization and nanobiointeractions with red blood cells and human plasma proteins, Appl. Surf. Sci. 437 (2018) 110–121, https://doi.org/10.1016/j.apsusc.2017.12.082.
[66] J. Yang, T. Wang, L. Zhao, V.K. Rajasekhar, S. Joshi, C. Andreou, S. Pal, H.T. Hsu, H. Zhang, I.J. Cohen, R. Huang, R.C. Hendrickson, M.M. Miele, W. Pei, M.B. Brendel, J.H. Healey, G. Chiosis, M.F. Kircher, Gold/alpha-lactalbumin nanoprobes for the imaging and treatment of breast cancer, Nat Biomed Eng 4 (2020) 686–703, https://doi.org/10.1038/s41551-020-0584-z.
[67] W. Xie, W.-W. Deng, M. Zan, L. Rao, G.-T. Yu, D.-M. Zhu, W.-T. Wu, B. Chen, L.-W. Ji, L. Chen, K. Liu, S.-S. Guo, H.-M. Huang, W.-F. Zhang, X. Zhao, Y. Yuan, W. Dong, Z.-J. Sun, W. Liu, Cancer cell membrane camouflaged nanoparticles to realize starvation therapy together with checkpoint blockades for enhancing cancer therapy, ACS Nano 13 (2019) 2849–2857, https://doi.org/10.1021/acsnano.8b03788.
[68] K. Wang, J. Lu, J. Li, Y. Gao, Y. Mao, Q. Zhao, S. Wang, Current trends in smart mesoporous silica-based nanovehicles for photoactivated cancer therapy, J. Contr. Release 339 (2021) 445–472, https://doi.org/10.1016/j.jconrel.2021.10.005.
[69] L.J. Feng Shuaipeng, Kaili Wang, Advances in smart mesoporous carbon nanoplatforms for photothermal–enhanced synergistic cancer therapy, Chem. Eng. J. 435 (2022) 134886.
[70] H.T. Sun, Q. Zhang, J.C. Li, S.J. Peng, X.L. Wang, R. Cai, Near-infrared photoactivated nanomedicines for photothermal synergistic cancer therapy, Nano Today 37 (2021) 29, https://doi.org/10.1016/j.nantod.2020.101073.
[71] J. Liu, C. Chen, T. Wei, O. Gayet, C. Loncle, L. Borge, N. Dusetti, X. Ma, D. Marson, E. Laurini, S. Pricl, Z. Gu, J. Iovanna, L. Peng, X.-J. Liang, Dendrimeric nanosystem consistently circumvents heterogeneous drug response and resistance in pancreatic cancer, Exploration 1 (2021) 21–34, https://doi.org/10.1002/EXP.20210003.
[72] H.-W. An, M. Mamuti, X. Wang, H. Yao, M.-D. Wang, L. Zhao, L.-L. Li, Rationally designed modular drug delivery platform based on intracellular peptide self-assembly, Exploration 1 (2021) 20210153, https://doi.org/10.1002/EXP.20210153.